Robotics and Computer Integrated Manufacturing 68 (2021) 102049

Contents lists available at ScienceDirect

Robotics and Computer Integrated Manufacturing

journal homepage: www.elsevier.com/locate/rcim

Direct method for updating flexible multibody systems applied to a milling robot

Hoai Nam Huynh[*,a], Hamed Assadi[b], Valentin Dambly[c], Edouard Rivière-Lorphèvre[d], Olivier Verlinden[c]

[a] Manufacturing Automation Laboratory, The University of British Columbia, Department of Mechanical Engineering, Vancouver, BC V6T 1Z4, Canada
[b] Faculty of Engineering, University of Victoria, Finnerty Road Engineering Office Wing 3800, Victoria BC V8P 5C2, Canada
[c] Theoretical Mechanics, Dynamics and Vibrations unit, University of Mons, Place du Parc 20, 7000 Mons, Belgium
[d] Machine Design and Production Engineering unit, University of Mons, Place du Parc 20, 7000 Mons, Belgium

ARTICLE INFO

Keywords:
Flexible multibody systems
Identification
Milling
Modal analysis
Model updating
Robotics

ABSTRACT

Industrial robots are currently used in light milling operations for their low cost and large workspace compared with CNC machine tools. However, milling robots are prone to vibration instabilities (chatter) and process deviations since they are significantly less stiff than machine tools. As a result, robot dynamic response depends on its posture which represents a major challenge. This paper presents a direct method to update any multibody model, enclosing flexible rotational/translational or virtual joints with minimal tuning. The novel method allows determining the elastic parameters of the model based on a curve fitting of the frequency response functions measured at the tool tip. Fitting is fast and efficient as it occurs in the frequency domain without the need to transform the measured data into the model parameter space. It relies on a genetic algorithm followed by a deterministic procedure to ensure a refined solution of the identified global minimum. The method is firstly demonstrated and validated on a simulated flexible manipulator with three rotational joints. Its multibody model is built using minimal coordinates with known elastic parameters that the method recovers accurately. The new fitting algorithm is eventually applied to an actual industrial robot (KUKA KR90 R3100 robotic arm) resulting in the proper fit of its critical resonances. Posture dependency can also be tackled by considering multiple measurements in different poses within the same fitting procedure. Updating procedure was programmed in Matlab and made public so that it can be easily adapted to identify elastic parameters of other flexible mechanical systems.

1. Introduction

In the context of Industry 4.0, factories are definitely oriented towards increasingly automated, flexible and connected production units, relying more and more on so-called digital twins [1,2]. Robotics and automation in manufacturing technologies are part of this 4^{th} industrial revolution [3]. In recent years, robotic machining gained in popularity from both academics and industrials. As a matter of fact, industrial manipulators, typically enclosing 6 axes, can cover larger workspace, reach narrow area on the workpiece and are far less expensive than machine tools. Furthermore, they can improve the productivity of actual manufacturing process thanks to easier set-up and portability. Besides, variety of material-removal processes can be carried out by switching the end-effectors or cutting tools [4]. Nevertheless, the downfall of using industrial robots for machining applications is that they are more prone to deviate from their trajectory and to experience self-excited vibrations. The reason is their extremely low stiffness relative to machine tools, hence limiting their scope in machining applications. Nowadays, robotic machining is limited to light milling operations such as deburring, polishing, grinding and material-removal on metal parts as long as the cutting forces remain relatively low [5–7]. Aeronautics and foundry industries are the main recipients of the technology for finishing operations on large parts and/or complex shapes [8].

A digital twin is a virtual model of an industrial process aiming at exhibiting the same dynamic behavior as its actual counterpart. Their use is profitable to design a machine, improve the performances, tune and validate controllers but also to monitor the process and react if

* Corresponding author
E-mail addresses: hoainam.huynh@ubc.ca (H.N. Huynh), hamedassadi@uvic.ca (H. Assadi), valentin.dambly@umons.ac.be (V. Dambly), edouard.rivierelorphevre@umons.ac.be (E. Rivière-Lorphèvre), olivier.verlinden@umons.ac.be (O. Verlinden).

https://doi.org/10.1016/j.rcim.2020.102049
Received 5 March 2020; Received in revised form 1 August 2020; Accepted 2 August 2020

necessary [9–11]. Considering robotic machining, the development of digital twins involves knowledge on robot kinematics, dynamics, control and milling process. While extensive research has been carried out in milling by Altintas et al. [12], there is still a long way to go before reaching a nearly-perfect fitted dynamic model of a robotic arm. For most of the robotic arms, their kinematics are straightforward and documented. However, before tuning the controllers, the generation and the updating of the robot dynamic model are still challenges to address [13,14]. Industrial robots are commonly modeled as a succession of rigid bodies connected by spring and damper pairs representing the joint flexibility. Rigid body inertia properties are usually determined from CAD (Computer-Aided Design) models or through rigid-body identification methods [15]. Sophisticated models treat the links as flexible bodies using beam elements updated through finite element models [16,17]. Determining the elastic parameters (stiffness and damping) of the spring and damper pairs is however challenging but critical to capture the robot dynamics. In fact, many studies reported that robot dynamics depend on their posture which is caused by a non linear joint stiffness and a changing mass distribution [18,19]. This effect is readily visible on the surface quality of machined parts when the end-effector sweeps a large workspace [20].

Focussing on the identification of the joint elastic parameters, researchers developed different approaches to update their robot dynamic model. Dumas et al. [21] proposed a robust and fast procedure to determine the joint stiffness around the axes of motion. The method is based on the application of translational forces and torques at the end effector while the axis deflections are measured by a laser tracker. Variants of the method relying on similar set-ups were developed allowing a precise joint stiffness characterization but require expensive equipment (i.e. laser scanner) [18,22–24]. Lehmann et al. [25] used the so-called clamping method to determine the joint stiffness of ABB IRB2400 robot. The robot end effector is clamped to a fixed force sensor and built-in encoders read the deflection on each axis. Mercère et al. handled the identification of varying parameters over the workspace using scheduling methods [26]. It is however known that such method is not viable in industry as it requires to measure all postures before interpolation. Even though the non linear stiffness behavior can be accurately captured using the aforementioned methods, dynamic properties, such as natural frequencies, dampings and mode shapes, are usually estimated using experimental modal analysis (EMA). Roving hammer technique is generally employed and consists in performing hammer impacts on the whole structure while vibrations are measured at the end effector [27]. Measured frequency response functions (FRFs) are then used to manually tune the elastic parameters around axes [28–31]. Nevertheless, as pointed out by Klimchik et al. [32], only considering the joint flexibility around the motion axes is not sufficient to fully capture the manipulator dynamics. Hence, they proposed the so-called Virtual Joint Model in which extra spring and damper pairs are appended in all directions, along and around each axis. Since estimating the characteristics of each spring and damper pair is very challenging, it is common to only include the torsional flexibilities. But still, elastic parameters were manually or semi-automatically identified on the basis of a fine and tedious tuning of the initial guess [33]. In [34], they are determined by using the measured values of natural frequencies and damping ratios without considering the mode shapes.

Therefore, in this paper, a direct method to update any flexible multibody dynamic (MBD) model, with rotational or translational joints, and determine its fitted elastic parameters (joint stiffness and damping) is presented and experimentally validated in one posture. A brief reminder on multibody modeling is presented in Section 2. The novel method is based on a frequency response function (FRF) curve fitting using a genetic algorithm followed by a deterministic procedure to refine the solution. In Section 3, the formulation of the method is detailed and immediately applied to an arbitrary manipulator as a validation example in Section 4. Following section covers a complete practical application of the updating method to a 6-axis industrial robot (KUKA KR90 R3100 HA) dedicated to milling operations. Its modal parameters (natural frequencies, damping ratios and mode shapes) are first identified through experimental modal analysis and the updating method is used to update the elastic coefficients of the joint torsional springs in all directions (Section 5). A discussion is eventually proposed on the identification of elastic coefficients to handle the posture-dependency problem. Concluding comments and future works are addressed in the conclusion section.

2. Multibody modeling

In this section, the kinematic and dynamic model of a multibody system gathering rigid bodies is derived using the generalized coordinates (i.e. minimal coordinates). In addition to the joint motions, elasticities between bodies are modeled using spring and damper pairs. The expressions of the equations of motion are derived knowing that the constitutive matrices will be used in the updating method to build the simulated frequency response functions.

2.1. Kinematic modeling

In rigid body dynamics, each body i is characterized by its mass m_i and its central tensor of inertia $\mathbf{\Phi}_{G,i}$ taken at its center of mass G_i. Opposed to the Cartesian coordinates, the multibody model encloses the minimum number of configuration parameters n_{cp} (i.e. degrees of freedom $\mathbf{q}$). They can be chosen arbitrarily as long as there is a one-to-one relationship with the configuration of the system. A main frame (i.e. coordinate system) usually locates the center of mass G_i of body i with respect to a fixed global reference frame whose origin is labelled 0. Note as well that body i can also gather one or multiple secondary frames labelled $i.j$ as illustrated in Figure 1, rigidly attached to body i through a constant homogeneous transformation matrix $\mathbf{T}_{i,\ i.j}$. For instance, the frame to which the sensor (i.e. accelerometer) is attached is a secondary frame.

The situation of each body is expressed using homogeneous transformation matrix $\mathbf{T}_{0,\ iy}(\mathbf{q})$ which provides the situation of main frame i with respect to reference frame 0 in terms of configuration parameter vector $\mathbf{q}$ such as

$$\mathbf{T}_{0,i}(\mathbf{q}) = \begin{bmatrix} \mathbf{R_{0,i}}(\mathbf{q}) & \{\mathbf{e_i}(\mathbf{q})\}_0 \\ \mathbf{000} & \mathbf{1} \end{bmatrix}, \tag{1}$$

where

- $\{\mathbf{e}_i(\mathbf{q})\}_0$ is the coordinate vector of frame i with respect to reference frame 0 and subscript 0 indicates that vector $\{\mathbf{e}_i(\mathbf{q})\}$ is projected in frame 0;
- $\mathbf{R}_{0,\ i}(\mathbf{q})$ is the rotation matrix expressing the orientation of frame i with respect to frame 0.

Four elementary homogeneous transformation matrices can be defined reflecting a single motion, i.e. a rotation around one axis ($\mathbf{T}_{rotx}(\alpha)$, $\mathbf{T}_{roty}(\alpha)$, $\mathbf{T}_{rotz}(\alpha)$) or a translation along the axes of the frame ($\mathbf{T}_{disp}(x, y, z)$) (Relationships 2 and 3),

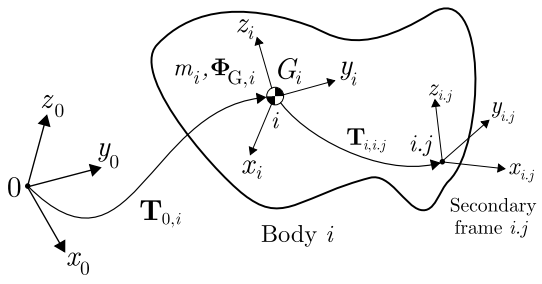

Fig. 1. Body reference frame

$$\mathbf{T}_{\text{disp}}(x,\,y,\,z) = \begin{bmatrix} 1 & 0 & 0 & x \\ 0 & 1 & 0 & y \\ 0 & 0 & 1 & z \\ 0 & 0 & 0 & 1 \end{bmatrix},\ \mathbf{T}_{\text{rotx}}(\alpha) = \begin{bmatrix} 1 & 0 & 0 & 0 \\ 0 & \cos(\alpha) & -\sin(\alpha) & 0 \\ 0 & \sin(\alpha) & \cos(\alpha) & 0 \\ 0 & 0 & 0 & 1 \end{bmatrix}, \tag{2}$$

$$\mathbf{T}_{\text{roty}}(\alpha) = \begin{bmatrix} \cos(\alpha) & 0 & \sin(\alpha) & 0 \\ 0 & 1 & 0 & 0 \\ -\sin(\alpha) & 0 & \cos(\alpha) & 0 \\ 0 & 0 & 0 & 1 \end{bmatrix} = \begin{bmatrix} \cos(\alpha) & -\sin(\alpha) & 0 & 0 \\ \sin(\alpha) & \cos(\alpha) & 0 & 0 \\ 0 & 0 & 1 & 0 \\ 0 & 0 & 0 & 1 \end{bmatrix}.$$
$$,\ \mathbf{T}_{\text{rotz}}(\alpha) \tag{3}$$

Complex motions can be achieved through the multiplication of the above elementary matrices using the following statement

$$\mathbf{T}_{i,k} = \mathbf{T}_{i,j}\cdot\mathbf{T}_{j,k}. \tag{4}$$

Translational and rotational velocities of frame i (or secondary frame $i.j$) are respectively denoted by $\boldsymbol{v}_i$ and $\boldsymbol{\omega}_i$ and are obtained via time differentiation of the homogeneous transformation matrices such as

$$\begin{aligned} \{\mathbf{v}_i\}_0 &= \sum_{j=1}^{n_{\text{cp}}} \frac{\partial\{\mathbf{e}_i\}_0}{\partial q_j}\cdot\dot{q}_j = [\mathbf{J}_{S,i}]_0\cdot\dot{\mathbf{q}}, \\ [\tilde{\omega}_i]_0 &= \sum_{j=1}^{n_{\text{cp}}} \frac{\partial\mathbf{R}_{0,i}}{\partial q_j}\cdot\mathbf{R}_{0,i}^{\text{T}}\cdot\dot{q}_j \rightarrow \{\boldsymbol{\omega}_i\}_0 = [\mathbf{J}_{\omega,i}]_0\cdot\dot{\mathbf{q}}, \end{aligned} \tag{5}$$

with $[\tilde{\omega}_i]_0$ a skew-symmetric matrix from which rotational velocities $\boldsymbol{\omega}_i$ can be retrieved. Skew-symmetric matrix $[\tilde{\omega}_i]_0$ reads

$$[\tilde{\omega}_i]_0 = \begin{bmatrix} 0 & -\omega_z & \omega_y \\ \omega_z & 0 & -\omega_x \\ -\omega_y & \omega_x & 0 \end{bmatrix}. \tag{6}$$

Acceleration expressions are obtained by time differentiation of velocity leading to translational and rotational accelerations, $\boldsymbol{a}_i$ and $\dot{\boldsymbol{\omega}}_i$, respectively. Entities $[\mathbf{J}_{S,\,i}]_0$ and $[\mathbf{J}_{\omega,\,i}]_0$ are known as the translational and rotational Jacobian matrices.

2.2. Equations of motion

The general form of the equations of motion is expressed as follows

$$\mathbf{M}_{\mathbf{q}}(\mathbf{q})\ddot{\mathbf{q}}(t) + \mathbf{C}_{\mathbf{q}}(\mathbf{q},\,\dot{\mathbf{q}})\dot{\mathbf{q}}(t) + \mathbf{K}_{\mathbf{q}}\mathbf{q}(t) = \mathbf{F}(t), \tag{7}$$

where $\mathbf{M}_{\mathbf{q}} \in \mathbb{R}^{n_{\text{cp}}\times n_{\text{cp}}}$, $\mathbf{C}_{\mathbf{q}} \in \mathbb{R}^{n_{\text{cp}}\times n_{\text{cp}}}$ and $\mathbf{K}_{\mathbf{q}} \in \mathbb{R}^{n_{\text{cp}}\times n_{\text{cp}}}$ denote the system mass, damping and stiffness matrices, respectively, and $\mathbf{F}(t) \in \mathbb{R}^{n_{\text{cp}}}$ the vector of applied forces. Subscript $\mathbf{q}$ indicates that constitutive matrices are expressed in the space of configuration parameters. Mass matrix $\mathbf{M}_{\mathbf{q}}$ is obtained using the Jacobian matrices such as

$$\mathbf{M}_{\mathbf{q}}(\mathbf{q}) = \sum_{i=1}^{n_{\text{B}}} (m_i[\mathbf{J}_{S,i}]_0^{\text{T}}\cdot[\mathbf{J}_{S,i}]_0 + [\mathbf{J}_{\omega,i}]_0^{\text{T}}\cdot\mathbf{R}_{0,i}\cdot[\boldsymbol{\Phi}_{G,i}]_i\cdot\mathbf{R}_{0,i}^{\text{T}}\cdot[\mathbf{J}_{\omega,i}]_0), \tag{8}$$

with n_{B} the number of bodies in the system.

According to the theorem of virtual power, Coriolis, gyroscopic and centrifugal forces are all gathered in term $\mathbf{C}_{\mathbf{q}}(\mathbf{q},\,\dot{\mathbf{q}})\dot{\mathbf{q}}$ whose expression is given by

$$\begin{aligned} \mathbf{C}_{\mathbf{q}}(\mathbf{q},\,\dot{\mathbf{q}})\dot{\mathbf{q}} = \sum_{i=1}^{n_{\text{B}}} (m_i[\mathbf{J}_{S,i}]_0^{\text{T}}\cdot[\dot{\mathbf{J}}_{S,i}]_0 + [\mathbf{J}_{\omega,i}]_0^{\text{T}}\cdot\mathbf{R}_{0,i}\cdot[\boldsymbol{\Phi}_{G,i}]_i\cdot\mathbf{R}_{0,i}^{\text{T}}\cdot[\dot{\mathbf{J}}_{\omega,i}]_0)\cdot\dot{\mathbf{q}} \\ + [\mathbf{J}_{\omega,i}]_0^{\text{T}}\cdot(\{\boldsymbol{\omega}_i\}_{\mathbf{0}} \times (\mathbf{R}_{0,i}\cdot[\boldsymbol{\Phi}_{G,i}]_i\cdot\mathbf{R}_{0,i}^{\text{T}})\{\boldsymbol{\omega}_i\}_0). \end{aligned} \tag{9}$$

Without considering stiffness matrix $\mathbf{K}_{\mathbf{q}}$, applied forces are expressed as follows

$$\mathbf{F} = \sum_{i=1}^{n_{\text{B}}} ([\mathbf{J}_{S,i}]_0^{\text{T}}\cdot\{\mathcal{R}_i\}_0 + [\mathbf{J}_{\omega,i}]_0^{\text{T}}\cdot\{\mathcal{M}_{G,i}\}_0), \tag{10}$$

with $\{\mathcal{R}_i\}_0$ the resultant of all translational forces applied on body i and $\{\mathcal{M}_{G,i}\}_0$ the resultant of all applied moments exerted on body i with respect to its center of mass, both projected in frame 0. Gravity vector $\mathbf{g}$ is introduced as an applied force on each main frame i such as

$$\{\mathcal{R}_i\}_0 = m_i\cdot\mathbf{g}. \tag{11}$$

Elastic forces can easily be introduced between frame i (action force) and frame j (reaction force) as long as stiffness k_{q_p} and damping d_{q_p} of each flexible element are known. In the case of torsional springs and dampers associated with the joints, the resultant moments read

$$\{\mathcal{M}_{G,i}\}_0 = \left(k_{q_p}\cdot\left(q_p^{Ref} - q_p\right) + d_{q_p}\cdot\left(\dot{q}_p^{Ref} - \dot{q}_p\right)\right)\cdot\mathbf{R}_{0,i}\cdot\mathbf{u}_{x,y,z}(\text{action}), \tag{12}$$

$$\{\mathcal{M}_{G,j}\}_0 = -\left(k_{q_p}\cdot\left(q_p^{Ref} - q_p\right) + d_{q_p}\cdot\left(\dot{q}_p^{Ref} - \dot{q}_p\right)\right)\cdot\mathbf{R}_{0,i}\cdot\mathbf{u}_{x,y,z}(\text{reaction}), \tag{13}$$

with $\mathbf{u}_{x,\,y,\,z}$ a unit vector selecting the column of the rotation matrix around which the torsional spring rotates (e.g. $\mathbf{u}_z = [0\ 0\ 1]^{\text{T}}$). For translational springs and dampers, same expressions are derived and enclosed in $\{\mathcal{R}_i\}_0$ for the action and in $\{\mathcal{R}_j\}_0$ for the reaction. Rest configuration of the multibody model is given by $\mathbf{q}_p^{Ref}$ and $\dot{\mathbf{q}}_p^{Ref}$ (e.g. for an industrial robot, q_p^{Ref} represents one of the joint axis angles in which EMA is performed, i.e. $\dot{\mathbf{q}}_p^{Ref} = 0$, typically). Similar expressions are derived in the case of translational springs and dampers. Unfortunately, elastic parameters in the configuration parameter space need to be determined from EMA (i.e. measured FRFs) tests and are enclosed in vector $\mathbf{p}_{\text{Elastic}} = [\mathbf{k}_q\ \mathbf{d}_q]^{\text{T}}$.

2.3. Linearized dynamic model

Equations of motion (Eq. 7) can be written into their residual form $\mathbf{f}$ such as

$$\mathbf{f}(\mathbf{q},\,\dot{\mathbf{q}},\,\ddot{\mathbf{q}}) = \mathbf{0} \equiv \mathbf{M}_{\mathbf{q}}\ddot{\mathbf{q}} + \mathbf{C}_{\mathbf{q}}\dot{\mathbf{q}} + \mathbf{K}_{\mathbf{q}}\mathbf{q} - \mathbf{F} = \mathbf{0}. \tag{14}$$

They are linearized with respect to a reference position, i.e. the posture of the studied mechanical system analysed using EMA. This equilibrium configuration is characterized by a set of configuration parameters $\mathbf{q}^{Ref}$ with $\dot{\mathbf{q}}^{Ref} = \ddot{\mathbf{q}}^{Ref} = \mathbf{0}$. Considering small variations of the configuration parameters and their time derivatives with respect to the reference configuration as

$$\mathbf{q} = \mathbf{q}^{Ref} + \Delta\mathbf{q},\ \dot{\mathbf{q}} = \dot{\mathbf{q}}^{Ref} + \Delta\dot{\mathbf{q}},\ \ddot{\mathbf{q}} = \ddot{\mathbf{q}}^{Ref} + \Delta\ddot{\mathbf{q}}, \tag{15}$$

the equations of motion can be linearized in the form

$$\mathbf{M}_{\mathbf{q}}^0\cdot\Delta\ddot{\mathbf{q}} + \mathbf{C}_{\mathbf{q}}^0\cdot\Delta\dot{\mathbf{q}} + \mathbf{K}_{\mathbf{q}}^0\cdot\Delta\mathbf{q} = \mathbf{0}, \tag{16}$$

with

$$\mathbf{M}_{\mathbf{q}}^0 = \mathbf{M}_{\mathbf{q}}(\mathbf{q}^{\text{Ref}}),\ \mathbf{C}_{\mathbf{q}}^0 = \frac{\partial\mathbf{f}}{\partial\dot{\mathbf{q}}}|_{\text{Ref}},\ \mathbf{K}_{\mathbf{q}}^0 = \frac{\partial\mathbf{f}}{\partial\mathbf{q}}|_{\text{Ref}}. \tag{17}$$

Elements $\mathbf{C}_{\mathbf{q}}^0$ and $\mathbf{K}_{\mathbf{q}}^0$ are called the tangent damping and stiffness matrices and are used to derive the natural frequencies, damping ratios and mode shapes of the multibody model. By introducing state vector $\Delta\mathbf{q}_{\text{u}} = [\Delta\mathbf{q}^{\text{T}}\ \Delta\dot{\mathbf{q}}^{\text{T}}]^{\text{T}}$, the linearized equations of motion (Eq. 16) are expressed in their first order form as

$$\hat{\mathbf{A}}\,\Delta\dot{\mathbf{q}}_u + \hat{\mathbf{B}}\,\Delta\mathbf{q}_u = \mathbf{0}, \tag{18}$$

$$\hat{\mathbf{A}} = \begin{bmatrix} \mathbf{C}_{\mathbf{q}}^0 & \mathbf{M}_{\mathbf{q}}^0 \\ \mathbf{M}_{\mathbf{q}}^0 & \mathbf{0} \end{bmatrix} \text{ and } \hat{\mathbf{B}} = \begin{bmatrix} \mathbf{K}_{\mathbf{q}}^0 & \mathbf{0} \\ \mathbf{0} & -\mathbf{M}_{\mathbf{q}}^0 \end{bmatrix}. \tag{19}$$

The simulated (subscript s) natural frequencies of the robot structure $f_{s,k}$, and associated simulated damping ratios $\zeta_{s,k}$, are obtained from the generalized eigenvalues $\lambda_{s,k}$ of matrices $\hat{\mathbf{A}}$ and $\hat{\mathbf{B}}$ such as

$$f_{s,k} = \frac{\mathrm{Im}(\lambda_{s,k})}{2\pi}[\mathrm{Hz}], \text{ and } \zeta_{s,k} = \frac{-\mathrm{Re}(\lambda_{s,k})}{\sqrt{\mathrm{Re}(\lambda_{s,k})^2 + \mathrm{Im}(\lambda_{s,k})^2}}. \quad (20)$$

3. Updating method

The proposed method is appropriate to achieve a model updating of any multibody system comprising flexible joints to determine suitable elastic parameters (joint stiffness and damping). The idea of the method is to perform a curve fitting in the sensor frame of the measured FRF matrix $\mathbf{H}(\omega)$ (generally composed of H_{xx}, H_{yy}, H_{zz}, H_{xy}, H_{xz}, H_{yx}, H_{yz}, H_{zx} and H_{zy}). In other words, measured FRFs are directly used without the need to transpose them in the configuration parameter space (joint coordinates). The method is said to be straightforward as the algorithm is supposed to deliver the optimum values for the sought parameters without manual tuning. Global minimum of the error function between the simulated and measured FRFs is ensured by a combination of genetic and deterministic algorithms. Each iteration of the genetic algorithm can be quickly completed since the simulated FRFs are computed in the frequency domain and in the joint space (configuration parameter space) of the manipulator before being transposed back to the sensor frame.

3.1. Cost function

From a general point of view, the dynamics of any mechanical system can be modeled using FRF matrix $\mathbf{H}(\omega)$ such as

$$\mathbf{H}(\omega) = (-\mathbf{M}\omega^2 + \mathbf{C}i\omega + \mathbf{K})^{-1}, \quad (21)$$

with complex variable i, mass matrix $\mathbf{M}$, damping matrix $\mathbf{C}$ and stiffness matrix $\mathbf{K}$ expressed in the Cartesian coordinates or sensor frame (e.g. typically accelerometer). Assuming that FRF matrix $\mathbf{H}(\omega)$ can be measured over a suitable frequency bandwidth to reveal the structural modes of the physical system and that its mass matrix $\mathbf{M}_\mathbf{q}^0(\mathbf{q}^{\mathrm{Ref}})$ is available (e.g. from CAD models), the proposed updating method is aimed at determining suitable elastic parameters in joint space $\mathbf{p}_{\mathrm{Elastic}} = [\mathbf{k}_q\ \mathbf{d}_q]^{\mathrm{T}}$ to optimally capture the dynamics measured by the sensor (i.e. FRFs). As a necessary requirement to successfully apply the curve fitting procedure, the multibody model must be composed of rigid bodies linked by an adequate number of elastic joints (rotational or translational) and located according to the measured mode shapes: for instance, one may add virtual spring and damper pairs between the ground and the mechanical system. In other words, the multibody model must be able to capture the targeted modes to fit. Once the design of the multibody model is achieved, the fitting algorithm can be deployed as explained below.

Elastic parameters $\mathbf{p}_{\mathrm{Elastic}}$ are determined such that they minimize the error between the measured and simulated FRFs in the sensor frame. The general idea is to simultaneously fit all the measured FRFs gathered in [3 × 3] matrix $\mathbf{H}(\omega)$, at one flexible point of the mechanical system (e.g. tool tip), with simulated FRFs from the multibody model. Each set is evaluated by submitting the iterated elastic parameters to the fitting procedure which computes the value of the cost function J as the summation of all errors between the measured and simulated FRFs in the sensor frame. Cost function J that minimizes the error between components of matrix $\mathbf{H}(\omega)$, i.e. measured $H_{ij}(\omega)$ and $\mathbf{H}_\mathrm{s}(\omega)$, i.e. simulated $H_{s,ij}(\omega)$ FRFs, is defined as

$$\mathrm{J} = \min_{\mathbf{p}_{\mathrm{Elastic}}} \sum_{\mathrm{i=x|y|z}} \sum_{\mathrm{j=x|y|z}} \sum_{\mathrm{k}=1}^{\mathrm{N}_\omega} (\log[\mathrm{H}_{s,ij}(\omega_\mathrm{k}, \mathbf{p}_{\mathrm{Elastic}})] - \log[\mathrm{H}_{ij}(\omega_\mathrm{k})])^* \cdot \mathrm{W}(\omega_\mathrm{k}) \cdot (\log[\mathrm{H}_{s,ij}(\omega_\mathrm{k}, \mathbf{p}_{\mathrm{Elastic}})] - \log[\mathrm{H}_{ij}(\omega_\mathrm{k})]), \quad (22)$$

where N_ω is the number of discretized lines in the measured frequency response function, $W(\omega_k)$ a weighting function (user defined) that magnifies values around peaks in the measured FRFs and superscript * denotes the conjugate transpose vector. A similar cost function is used by Neubauer et al. in [35] for the fitting of FRFs in the joint space of a manipulator.

Simulated FRFs $H_{s,ij}(\omega)$ in the sensor coordinate system are derived from the equations of motion of the multibody model depending on configuration parameters $\mathbf{q}^{\mathrm{Ref}}$ and elastic parameters $\mathbf{p}_{\mathrm{Elastic}}$. Once the constitutive system matrices ($\mathbf{M}_\mathbf{q}^0$, $\mathbf{C}_\mathbf{q}^0$, $\mathbf{K}_\mathbf{q}^0$) are computed in a chosen reference configuration ($\mathbf{q}^{\mathrm{Ref}}$) for the manipulator, simulated FRFs $H_{s,ij}(\omega)$ can be derived by transposing them from the manipulator joint space to the sensor frame (usually a Cartesian frame). Homogeneous transformation matrix locating and orienting the sensor frame $\mathbf{T}_{0,\ \mathrm{Sensor}}(\mathbf{q}^{\mathrm{Ref}})$ is expressed in the reference frame using the direct kinematics, thus defining coordinate vector $\{\mathbf{e}_{\mathrm{Sensor}}(\mathbf{q}^{\mathrm{Ref}})\}_0$ and rotation matrix $\mathbf{R}_{0,\ \mathrm{Sensor}}(\mathbf{q}^{\mathrm{Ref}})$. A virtual experimental modal analysis is then performed by applying force F_{EMA} at the sensor frame in the direction of excitation j, representing one of the directions x, y or z, such as

$$\{\mathbf{F}_{\mathrm{Sensor},j}\}_0 = F_{\mathrm{EMA}} \cdot \mathbf{R}_{0,\mathrm{Sensor}} \cdot \{\mathbf{u}_j\}_{\mathrm{Sensor}}. \quad (23)$$

Applied force is projected in the reference frame and then converted into the vector of joint torques (forces) $\boldsymbol{\tau}_j$ using the translational component of the geometric Jacobian matrix $[\mathbf{J}_{\mathrm{S},\ \mathrm{Sensor}}]_0$ of the sensor and projected in the reference frame such as

$$\boldsymbol{\tau}_j = [\mathbf{J}_{\mathrm{S,Sensor}}]_0^{\mathrm{T}} \cdot \{\mathbf{F}_{\mathrm{Sensor},j}\}_0. \quad (24)$$

The resulting variations in the degrees of freedom $d\mathbf{q}$, which are complex values, corresponding to joint torque $\boldsymbol{\tau}_j$ are computed at each frequency ω_k using the linearized matrices as follows

$$d\mathbf{q}(\omega_k)_j = (-\mathbf{M}_\mathbf{q}^0\omega_k^2 + \mathbf{C}_\mathbf{q}^0(\mathbf{p}_{\mathrm{Elastic}})i\omega_k + \mathbf{K}_\mathbf{q}^0(\mathbf{p}_{\mathrm{Elastic}}))^{-1}\boldsymbol{\tau}_j. \quad (25)$$

Linearized damping $\mathbf{C}^0(\mathbf{p}_{\mathrm{Elastic}})$ and stiffness $\mathbf{K}^0(\mathbf{p}_{\mathrm{Elastic}})$ matrices depend on the elastic parameters which are iterated throughout the fitting process. Variations in the pose of the sensor are computed as the difference between the pose considering the applied force and the reference sensor pose which are transposed back in the sensor frame such as

$$\{\mathrm{Re}(\Delta\mathbf{e}_j)\}_{\mathrm{Sensor}} = \mathbf{R}_{0,\mathrm{Sensor}}^{-1} \cdot (\{\mathbf{e}(\mathbf{q}^{\mathrm{Ref}} + \mathrm{Re}(d\mathbf{q}(\omega_k)_j))_{\mathrm{Sensor}}\}_0 - \{\mathbf{e}(\mathbf{q}^{\mathrm{Ref}})_{\mathrm{Sensor}}\}_0), \quad (26)$$

$$\{\mathrm{Im}(\Delta\mathbf{e}_j)\}_{\mathrm{Sensor}} = \mathbf{R}_{0,\mathrm{Sensor}}^{-1} \cdot (\{\mathbf{e}(\mathbf{q}^{\mathrm{Ref}} + \mathrm{Im}(d\mathbf{q}(\omega_k)_j))_{\mathrm{Sensor}}\}_0 - \{\mathbf{e}(\mathbf{q}^{\mathrm{Ref}})_{\mathrm{Sensor}}\}_0). \quad (27)$$

Simulated FRFs are constructed using coordinate vectors $\mathrm{Re}(\Delta\mathbf{e}_j)$ and $\mathrm{Im}(\Delta\mathbf{e}_j)$ projected in the sensor frame for each frequency (ω_k) such as

$$\begin{bmatrix} \mathrm{H}_{s,xj}(\omega_\mathrm{k}) \\ \mathrm{H}_{s,yj}(\omega_\mathrm{k}) \\ \mathrm{H}_{s,zj}(\omega_\mathrm{k}) \end{bmatrix} = \frac{1}{\mathrm{F}_{\mathrm{EMA}}}(\{\mathrm{Re}(\Delta\mathbf{e}_\mathrm{j})\}_{\mathrm{Sensor}} + \mathrm{i}\{\mathrm{Im}(\Delta\mathbf{e}_\mathrm{j})\}_{\mathrm{Sensor}}). \quad (28)$$

The nine simulated FRFs at the TCP, forming FRF matrix $\mathbf{H}_\mathbf{s}(\omega)$, are derived by successively applying force F_{EMA} along the x, y and z directions in Eq. 23. Cost function J is eventually evaluated by using measured FRFs $\mathbf{H}(\omega)$ at the sensor frame and simulated FRFs $\mathbf{H}_\mathbf{s}(\omega)$ in Eq. 22.

3.2. Fitting procedure

The fitting procedure relies on multiple runs of a genetic algorithm followed by a deterministic algorithm (Figure 2). Inputs of the algorithm are the measured FRFs and the multibody model under the form of constitutive matrices $\mathbf{M}_\mathbf{q}^0$, $\mathbf{C}_\mathbf{q}^0$, $\mathbf{K}_\mathbf{q}^0$ in the reference configuration $\mathbf{q}^{\mathrm{Ref}}$. Fitting procedure also has its own parameters such as fitness tolerance δ (relative error between two successive estimates of the function), size of population $S_{\mathrm{Pop.}}$ and number of generations $n_{\mathrm{Gen.}}$. Initial values of $\mathbf{p}_{\mathrm{Elastic}}$ can also be defined but are not mandatory since the genetic algorithm is able to generate a random initial population (i.e. multiple sets of $\mathbf{k}_q$ and $\mathbf{d}_q$). The initial population of $\mathbf{p}_{\mathrm{Elastic}}$ is built by using a

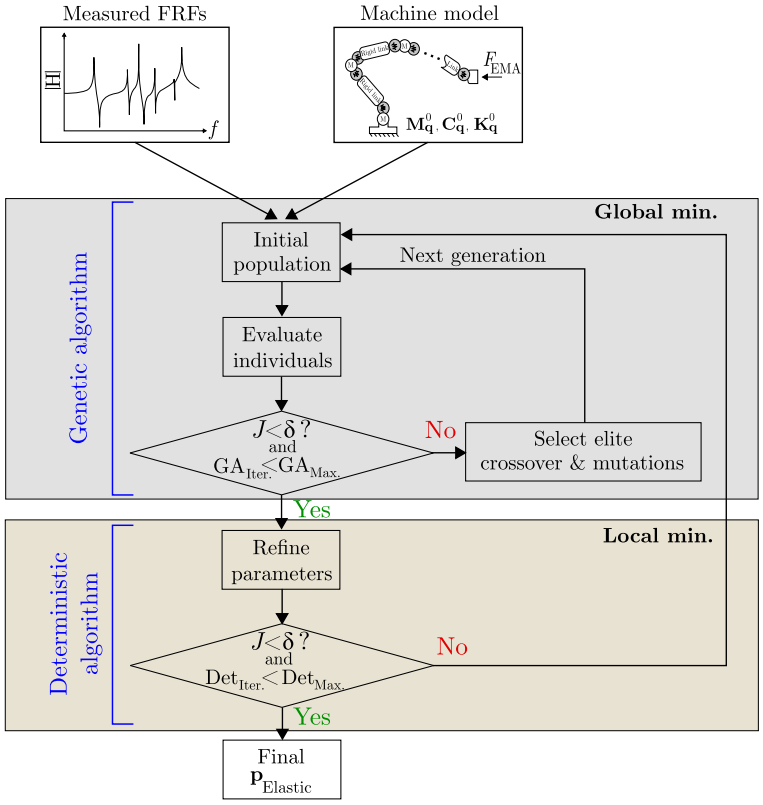

Fig. 2. Flowchart of the fitting procedure

uniform distribution around an initial (if provided) or random guess of elastic parameters. Maximum and minimum values for $\mathbf{k}_q$ and $\mathbf{d}_q$ can be specified to limit the search domain keeping in mind that they must be strictly positive to ensure a physical meaning.

Once the initial population constructed, the genetic algorithm starts to evaluate all individuals by computation of cost function J. If its value becomes lower than fitness tolerance δ, the deterministic algorithm takes over. Another common stopping criterion consists in specifying a stalling limit. However, most of time, the genetic algorithm stops because the maximum number of iterations is reached ($GA_{max.} = n_{Gen.} \cdot S_{Pop.}$). Otherwise, the genetic algorithm selects individuals that performed well and crosses and mutates them to create the next population. Anyway, the advantage of using genetic algorithm is its ability to find a global minimum in cost function J while the deterministic algorithm refines the solution by finding a local minimum. In the case that cost function J becomes lower than fitness tolerance δ, algorithm stops as a satisfactory set of elastic parameters is found. Otherwise, if the number of iterations for the deterministic algorithm is exceeded ($Det_{Iter.} > Det_{Max.}$) another genetic algorithm is started taking the final set $\mathbf{p}_{Elastic}$ resulting from the deterministic algorithm as initial values.

Deterministic algorithm uses the same cost function as the genetic algorithm (Eq. 22). It allows efficient and rapid refining of the values of elastic parameters to further minimize the value of the cost function in the curve fitting process. An implementation of the genetic algorithm can be found in Matlab under toolbox *GA* (requires the *Optimization* toolbox) as well as a deterministic algorithm with function *fminsearch*(). The latter implements the Nelder-Mead simplex direct algorithm [36].

4. Validation example

A validation example of model updating is provided for an arbitrary manipulator comprising three revolute joints. Joint flexibility is only considered around the three motion axes ($n_{cp} = 3$) and imposed joint stiffnesses and dampings are shown in Table 1. The aim of the validation example is to find back the six imposed elastic parameters by using the presented updating method. They lead to the 6 following modal parameters: $f_1 = 10.17$ Hz, $\zeta_1 = 1.89$ %, $f_2 = 11.24$ Hz, $\zeta_2 = 1.8$ %, $f_3 = 22.6$ Hz and $\zeta_3 = 1.66$ %.

The manipulator, illustrated in Figure 3, is geometrically characterized by the length of its first two links such as $a_1 = 0.35$ m and $a_2 = 1.35$ m. The homogeneous transformation matrices providing the pose of all centers of mass and the sensor frame can be computed by using relationships 29 to 32. The dynamics of the manipulator correspond to the values of inertial parameters proposed in Table 2. Components of inertia tensor $\mathbf{\Phi}_{G,i}$ are denoted by ϕ_G and vector coordinates of center of mass of body i are given with respect to the joint frame by (C_{xi}, C_{yi}, C_{zi}). For the sake of simplicity, note that the manipulator does not comprise any motor and degree of freedom $q_{z,i}$ represents the joint deflection around the motion axis (i.e. rotation around z-axis of the local frame).

$$\mathbf{T}_{0,1} = \mathbf{T}_{\text{rotz}}(q_{z,1}) \cdot \mathbf{T}_{\text{disp}}(C_{x_1}, C_{y_1}, C_{z_1}). \tag{29}$$

$$\mathbf{T}_{0,2} = \mathbf{T}_{0,1} \cdot \mathbf{T}_{\text{disp}}(a_1 - C_{x_1}, -C_{y_1}, -C_{z_1}) \cdot \mathbf{T}_{\text{rotx}}\left(\frac{\pi}{2}\right) \cdot \mathbf{T}_{\text{rotz}}(q_{z,2}) \cdot \mathbf{T}_{\text{disp}}(C_{x_2}, C_{y_2}, C_{z_2}). \tag{30}$$

Table 1
Selected joint stiffnesses and dampings for an arbitrary flexible multibody system

Joint stiffness [Nm/rad]	Joint damping [Nm.s/rad]
$k_{z,1}$	$d_{z,1}$
$2.0e^6$	$1.2e^3$
$k_{z,2}$	$d_{z,2}$
$3.0e^6$	$1.545e^3$
$k_{z,3}$	$d_{z,3}$
$1.55e^6$	$0.34e^3$

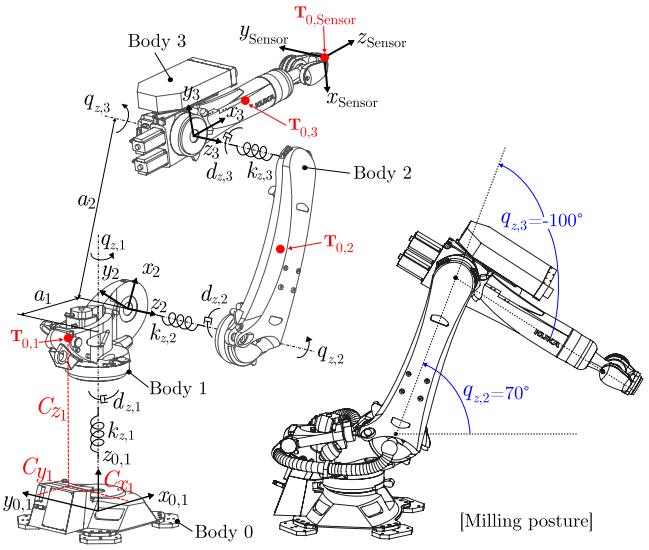

Fig. 3. Arbitrary flexible multibody model

Table 2
Inertia properties of the arbitrary flexible multibody system

	Body 1	Body 2	Body 3
m_i [m]	511.726	249.53	222.659
C_{x_i} [m]	-0.018	0.532	0.423
C_{y_i} [m]	0.002	-0.007	0.018
C_{z_i} [m]	-0.21	0.248	-0.018
ϕ_{G,xx_i} [kg.m^2]	19.45	5.014	5.882
ϕ_{G,yy_i} [kg.m^2]	33.893	57.621	49.927
ϕ_{G,zz_i} [kg.m^2]	30.242	56.853	48.9
ϕ_{G,xy_i} [kg.m^2]	2.274	-1.058	-1.372
ϕ_{G,xz_i} [kg.m^2]	0.938	5.498	0.074
ϕ_{G,yz_i} [kg.m^2]	0.373	-0.069	-1.202

$$\mathbf{T}_{0,3} = \mathbf{T}_{0,2}\cdot\mathbf{T}_{\text{disp}}(a_2 - C_{x_2}, -C_{y_2}, -C_{z_2})\cdot\mathbf{T}_{\text{rotz}}(q_{z,3})\cdot\mathbf{T}_{\text{disp}}(C_{x_3}, C_{y_3}, C_{z_3}). \tag{31}$$

$$\mathbf{T}_{0,\text{Sensor}} = \mathbf{T}_{0,3}\cdot\mathbf{T}_{\text{disp}}(1.566 - C_{x_3}, 0.042 - C_{y_3}, 0.005 - C_{z_3})\cdot\mathbf{T}_{\text{rotx}}\left(\frac{-\pi}{2}\right). \tag{32}$$

Elastic parameters are fitted in the following manipulator configuration $\mathbf{q}^{\text{Ref}}$: $q_{z,1} = 0^\circ$, $q_{z,2} = 70^\circ$ and $q_{z,3} = -100^\circ$. It is a typical posture used for milling applications hereafter called the *milling posture*. In this configuration and with the set of elastic parameters proposed in Table 1, values of linearized system matrices read

$$\mathbf{M}_{\mathbf{q}}^{0} = \begin{bmatrix} 482.1 & -30.5 & 0.3 \\ -30.5 & 588.8 & 72.1 \\ 0.3 & 72.1 & 88.7 \end{bmatrix}, \mathbf{C}_{\mathbf{q}}^{0} = \begin{bmatrix} 1200 & -0.01 & 0 \\ 0.35 & 1545 & 0.13 \\ -0.07 & -0.13 & 340 \end{bmatrix}, \tag{33}$$

$$\mathbf{K}_{\mathbf{q}}^{0} = \begin{bmatrix} 2e^6 & 0 & 0 \\ 0 & 3e^6 & 427.816 \\ 0 & 427.816 & 1.55e^6 \end{bmatrix}. \tag{34}$$

Using the presented updating method, parameters of the genetic algorithm are chosen as follows with a number of generations of $n_{\text{Gen.}} = 15$, a population size of $S_{\text{Pop.}} = 80$ (number of joint stiffness and damping sets evaluated during each generation) and a fitness tolerance of $\delta = 1e^{-12}$ (can be increased if one does not desire that the genetic algorithm stops after reaching $\text{GA}_{\text{Max.}}$). Number of generations and population size must naturally be increased if more elastic parameters are fitted and practical methods to tune genetic algorithm can be found in [37]. For the deterministic algorithm, the maximum number of iterations is fixed at $\text{Det}_{\text{Max.}} = 5000$ (too large in this case as observed in Figure 5 but difficult to guess). Initial values for $\mathbf{p}_{\text{Elastic}}$ are chosen randomly as far as they are strictly positive and in a reasonable range for stiffness and damping. FRFs to fit, normally measured from the actual machine, are generated by using the imposed elastic parameters and are hereafter called *pseudo-measured FRFs*. It leads to frequency response function matrix $\boldsymbol{H}(\omega)$ of the three structural modes in the sensor frame. Each FRF is sampled at $\Delta f = 0.2$ Hz over a bandwidth of 30 Hz. Selection of the bandwidth, i.e. modal parameters of the example, is made on the basis of actual measurements on an industrial robot [34]. Note that the inertance format ([m/s^2/N]) is deliberately chosen as it was observed that high frequency peaks are fitted more quickly as they clearly appear. Finally, weighting function $W(\omega_k)$ in Eq. 22 magnifies the values of FRFs around the peaks as highlighted in Figure 4. Using a peak-picking method, weights are set to a gain of 50 at each peak and also at $\pm\ 2\,\Delta f$ around each peak; gain is 0.5 on the rest of the frequency domain (weights can also be defined manually for each FRF). Once the genetic algorithm initialized, iterations are completed by following the steps described in Figure 2 using Eqs. 23 to 28.

After the completion of proposed updating method, simulated and pseudo-measured FRF curves in the sensor frame are almost not discernible. Sought joint stiffness and damping parameters are recovered with a negligible error. Following the set 1200 iterations of the genetic algorithm, it takes about 200 iterations for the deterministic algorithm to converge (vary upon the random results of genetic algorithm). Matlab default values for the genetic algorithm are applied for crossovers and mutations. The evolution of the corresponding cost function is depicted in Figure 5. As witnessed, process is indeed convergent since the value of the cost function starting at around 2e^5 m/s^2/N stabilizes around 1e^3 m/s^2/N thanks to the genetic algorithm. The deterministic algorithm eventually drops the cost function value near zero ($\simeq$ 1e^{-7} m/s^2/N). Proposed method is fast as convergence is reached in about 4 minutes using an Intel i7-8750H processor on the model updating example. Video of the FRF curve fitting is available through the following link https://youtu.be/riPu9QQl7dM as well as Matlab simulation files. They also include an extension of this example in which FRFs from different postures are fed to the fitting method slightly improving the convergence.

5. Industrial application

The updating method is applied to industrial robot KUKA KR90 R3100. An experimental modal analysis was performed in the milling posture ($q_{z,1} = 0^\circ$, $q_{z,2} = 70^\circ$ and $q_{z,3} = -100^\circ$) and experimental results are detailed in [34]. A tri-axis accelerometer located at the end-effector collected the direct FRFs from tap tests with a frequency resolution of 0.5 Hz. Four modes were measured in the milling posture below 30 Hz. Referring to Figure 6, mode one ($f_1 = 10.0$ Hz, $\zeta_1 = 1.4$ %) is mainly dominated by the stiffness of joint one around its motion axis ($q_{z,1}$). Mode two ($f_2 = 11.0$ Hz, $\zeta_2 = 1.0$ %) is formed by the deflection of the second joint of the robot around its axis of motion ($q_{z,2}$). Mode four ($f_4 = 23.7$ Hz, $\zeta_4 = 0.8$ %) is also greatly influenced by a rotation around an axis of motion, the third axis ($q_{z,3}$). However, for mode three ($f_3 = 19.2$ Hz, $\zeta_3 = 0.5$ %), it mostly involves the combination of rotations around the first joint about the axis of motion ($q_{z,1}$) but also **normal** to the axis of motion ($q_{x,1}$).

In order to capture all modes using the multibody approach, the Virtual Joint Model [32] is deployed by appending two extra torsional springs and dampers (not represented in Figure 6) orthogonal to the z-axis of each joint frame. It will allow simulating mode three at $f_3 = 19.2$ Hz involving a mode shape leading to a rotation around $q_{x,1}$. Since mode shapes only suggest deflections around the first three axes of Kuka robot, its dynamic model is limited to the first three joints. The manipulator was modeled with nine configuration parameters ($n_{\text{cp}} = 9$) as deflections may appear around any axis (actual or virtual) of the joint, in the most general case (using 4 configuration parameters, the

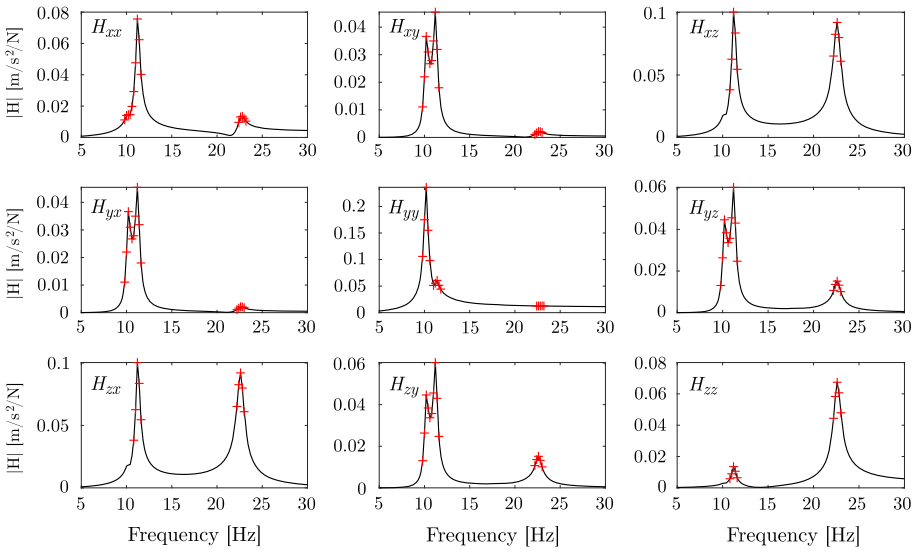

Fig. 4. Weighting of peaks of interest in the FRF matrix $\boldsymbol{H}(\omega)$ in inertance format

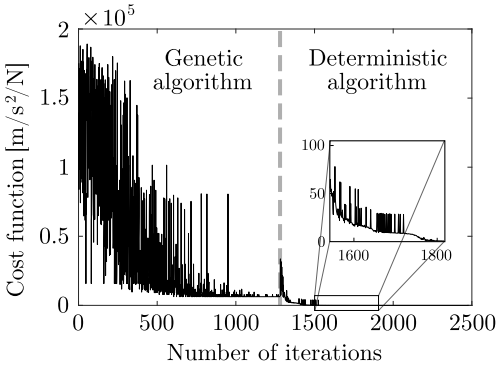

Fig. 5. Evolution of the cost function for the FRF fitting applied to the arbitrary flexible multibody system

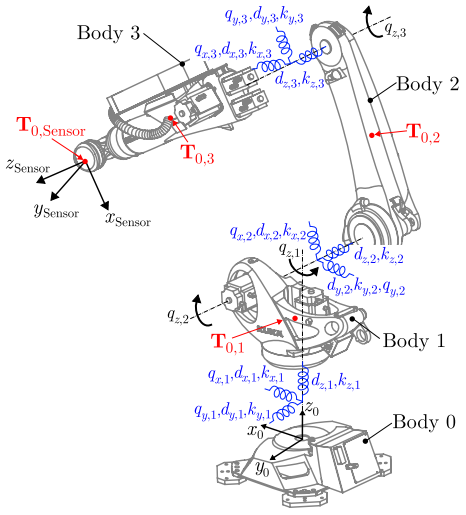

Fig. 6. Multibody model of KUKA R3100 with 3 torsional springs/dampers per joint

updating method is also able to quickly fit the 4 modes at the expense of a slight drop in accuracy). Only the fitting of elastic parameters is addressed in this paper since the inertia properties of the first three links were identified in [34] using a combination of rigid-body identification and CAD models. Identified inertia properties are enclosed in Table 3.

The homogeneous transformation matrices locating the centers of mass of each body are shown from Eq. 35 to 38. The links lengths are as follows: $a_1 = 0.35$ m and $a_2 = 1.35$ m.

$$\mathbf{T}_{0,1} = \mathbf{T}_{\text{rotz}}(q_{z,1})\cdot\mathbf{T}_{\text{rotx}}(q_{x,1})\cdot\mathbf{T}_{\text{roty}}(q_{y,1})\cdot\mathbf{T}_{\text{disp}}(C_{x_1}, C_{y_1}, C_{z_1}). \tag{35}$$

$$\mathbf{T}_{0,2} = \mathbf{T}_{0,1}\cdot\mathbf{T}_{\text{disp}}(a_1 - C_{x_1}, -C_{y_1}, -C_{z_1})\cdot\mathbf{T}_{\text{rotx}}\left(\frac{\pi}{2}\right)\cdot \mathbf{T}_{\text{rotz}}(q_{z,2})\cdot\mathbf{T}_{\text{rotx}}(q_{x,2})\cdot\mathbf{T}_{\text{roty}}(q_{y,2})\cdot\mathbf{T}_{\text{disp}}(C_{x_2}, C_{y_2}, C_{z_2}). \tag{36}$$

$$\mathbf{T}_{0,3} = \mathbf{T}_{0,2}\cdot\mathbf{T}_{\text{disp}}(a_2 - C_{x_2}, -C_{y_2}, -C_{z_2})\cdot\mathbf{T}_{\text{rotz}}(q_{z,3})\cdot \mathbf{T}_{\text{rotx}}(q_{x,3})\cdot\mathbf{T}_{\text{roty}}(q_{y,3})\cdot\mathbf{T}_{\text{disp}}(C_{x_3}, C_{y_3}, C_{z_3}). \tag{37}$$

$$\mathbf{T}_{0,\text{Sensor}} = \mathbf{T}_{0,3}\cdot\mathbf{T}_{\text{disp}}(1.566 - C_{x_3}, 0.042 - C_{y_3}, 0.005 - C_{z_3})\cdot\mathbf{T}_{\text{rotx}}\left(\frac{-\pi}{2}\right). \tag{38}$$

For the sake of performance evaluation of the updating method, three cases are considered to fit the 18 elastic parameters (stiffness and damping):

1. Fit on modeled FRFs: the elastic parameters of the multibody model are fitted on the FRFs computed on the basis of the identified joint stiffness and damping presented in [34].
2. Fit on measured FRFs: the parameters are identified on the raw measured FRFs.
3. Fit on synthesized FRFs: they are determined on reconstructed FRFs from EMA software.

Table 3
Inertia properties of the Kuka robot model

	Body 1	Body 2	Body 3
m_i [kg]	511.726	249.53	222.659
C_{x_i} [m]	-0.02	0.53	0.42
C_{y_i} [m]	0.0	0.0	0.02
C_{z_i} [m]	-0.21	0.25	-0.02
ϕ_{G,xx_i} [kg.m^2]	15.45	80.01	45.88
ϕ_{G,yy_i} [kg.m^2]	30.90	150.62	125.93
ϕ_{G,zz_i} [kg.m^2]	30.24	150.85	125.90
ϕ_{G,xy_i} [kg.m^2]	1.87	-1.06	-1.37
ϕ_{G,xz_i} [kg.m^2]	0.94	0.5	0.07
ϕ_{G,yz_i} [kg.m^2]	0.37	-0.07	-1.20

Table 4
Initial, maximum and minimum values for elastic parameters

Stiffness	Initial	Min.	Max.	Damping	Initial	Min.	Max.
$k_{z,1}$ [Nm/rad]	$3e^6$	$5.5e^5$	$5e^6$	$d_{z,1}$ [Nm.s/rad]	100	1	$1e^4$
$k_{x,1}$ [Nm/rad]	$4e^6$	$5.5e^5$	$5e^7$	$d_{x,1}$ [Nm.s/rad]	100	1	$1e^4$
$k_{y,1}$ [Nm/rad]	$8e^6$	$5.5e^5$	$5e^7$	$d_{y,1}$ [Nm.s/rad]	100	1	$1e^4$
$k_{z,2}$ [Nm/rad]	$4e^6$	$5.5e^5$	$8e^6$	$d_{z,2}$ [Nm.s/rad]	100	1	$1e^4$
$k_{x,2}$ [Nm/rad]	$8e^6$	$5.5e^5$	$4e^7$	$d_{x,2}$ [Nm.s/rad]	100	1	$1e^4$
$k_{y,2}$ [Nm/rad]	$4e^6$	$5.5e^5$	$4e^7$	$d_{y,2}$ [Nm.s/rad]	100	1	$1e^4$
$k_{z,3}$ [Nm/rad]	$1e^6$	$5.5e^5$	$4e^6$	$d_{z,3}$ [Nm.s/rad]	100	1	$1e^4$
$k_{x,3}$ [Nm/rad]	$5e^6$	$5.5e^5$	$1e^8$	$d_{x,3}$ [Nm.s/rad]	100	1	$1e^4$
$k_{y,3}$ [Nm/rad]	$8e^6$	$5.5e^5$	$1e^8$	$d_{y,3}$ [Nm.s/rad]	100	1	$1e^4$

Next subsections detail the fitting results and compare the performances. For all the three cases, the same guess and minimum and maximum values of elastic parameters are chosen as presented in Table 4. Mainly the maximum values of stiffness require some adjustment knowing that normal stiffnesses ($k_{x,i}$ and $k_{y,i}$) are higher than rotational stiffness ($k_{z,i}$). Besides, for most of 6-axis industrial robots, $k_{z,1}$ rules stiffness of the first mode corresponding to a rotation around the first motion joint. A initial guess can therefore be easily obtained by considering the first FRF peak. The number of generations is increased to $n_{\text{Gen.}}=20$ and the number of populations to $S_{\text{Pop.}}=100$ for a fitness tolerance of $\delta=300$. For the deterministic algorithm, the maximum number of iterations is fixed at $\text{Det}_{\text{Max.}}=10000$. FRFs are also fitted over a bandwidth of 30 Hz in the inertance format exhibiting higher amplitudes as the frequency increases. Weighting function $W(\omega_k)$ magnifies peaks and also $\pm$ 2 Δf around with a gain of 80; gain is 0.5 elsewhere (weights must be hand-selected for measured FRFs due to measurement noise). Genetic and deterministic algorithms are run according to Figure 2 using Eqs. 23 to 28.

5.1. Fit on modeled FRFs

The joint stiffnesses and dampings from [34] are adopted to generate the pseudo-measured FRFs to fit by using the presented multibody model Eqs. 35 to 38. Pseudo-measured FRFs are sampled at 0.2 Hz. After 17101 iterations, the updating method converges to an error below the fitness tolerance Figure 7 and 8 compares the fitted FRF matrix $\mathbf{H}(\omega)$ in amplitude (thick red line) against the raw measurements (thin black line) and the modeled FRFs from [34] (dotted blue line). Fitted FRFs are non discernible from the modeled FRFs. However, fitted parameters are different as explained later in Subsection 5.4 in Table 5. Again, the updating method is able to successfully curve fit the pseudo-measured FRFs even if the number of configuration parameters was increased.

To obtain this result, three successive runs of genetic and deterministic algorithms were necessary and completed in 2210 s to progressively reduce the stabilized value of the cost function. Its highest value of $2.65e^5$ [m/s^2/N] was reduced to 64 [m/s^2/N]. Note the chaotic behavior of the cost function during the evaluations of the genetic algorithm since random mutations of the sets of elastic parameters are performed (convergent value of 130 [m/s^2/N] for the cost function is attained in one run using a frequency resolution of 0.5 Hz without loosing accuracy in the fitting).

5.2. Fit on measured FRFs

Since fitted frequency peaks do not exactly match with the measured ones in Figure 7, one may wonder if results are improved when the updating method relies on raw FRF measurements. As a matter of fact, raw measured FRFs exhibit non linear behavior (amplitude is force dependent on tap testing) and non symmetric cross-FRFs. Using the frequency resolution of measured FRFs (0.5 Hz), the curve fitting was processed over more than 400,000 iterations (about 12 hours of simulation) and then stopped by the user since the cost function could not decrease below fitness tolerance δ (implemented routine allows user to save data every x iteration).

Resulting curve-fitted FRFs are compared to the raw FRFs in Figure 9. Although H_{xx} and H_{zz} show an acceptable level of fitting, for H_{yy}, the first peak at 10 Hz is not correlated even though boundaries were imposed for $k_{z,1}$. As iterations go by, it can also be observed that peaks become sharper announcing a potential error on the joint dampings. Moreover, since the multibody model is linear, the non symmetric cross-FRFs cannot be captured. Overall, the fitting is quite poor on this particular system because mode 1 (10 Hz) and mode 2 (11 Hz) are close. Better results can be expected on well-separated modes with less non-linearities.

5.3. Fit on synthesized FRFs

For the reason that the multibody model is linear, the last studied case is based on the curve fitting of the reconstructed FRFs from an experimental modal analysis software (LMS Test.Lab Rev. 8A). Once the FRFs are measured, time domain method Least Squares Complex Exponential (LSCE) was deployed to extract the modal parameters of industrial robot KUKA KR90 R3100 in [34]. Using the software modal parameters, LMS is able to reconstruct (synthesize) the measured FRFs using a modal space model. Figure 10 compares the fitted (thick red line), synthesized (dotted blue line) and raw measured FRFs (thin black line) using a frequency resolution of 0.5 Hz. Again, since the multibody model is linear, it cannot capture non-symmetric cross-FRFs. Therefore, user needs to select cross-FRFs and mirror for the counterparts (e.g. selection of H_{xy} and replacement of H_{yx} by H_{xy}). Another choice would consist in averaging cross-FRFs pairs.

After about 150,000 iterations (about 4 hours of simulation), the multibody model was able to capture all the frequency peaks with a coherent damping using the proposed updating method. In Figure 10, it can be observed that the fitting of cross-FRFs is less accurate (H_{xy} and H_{xz}) probably because the amplitude was low compared with the direct FRFs.

5.4. Comparison of fitting performances

All three curve fits are finally compared together. Firstly, the fitted elastic parameters are examined in Table 5 for all the studied cases. They are also compared to the ones semi-automatically fitted from [34]. It can be observed that although fitted FRFs and modeled from [34] were on top of each other, some differences arise. It is due to the fact that only four modes out of nine ($n_{\text{CP}}=9$) are fitted leaving the solution undetermined. It is generally the case in experimental modal analysis when the structure is excited over a certain frequency bandwidth and the FRFs are only able to capture a subset of modes. It also means that fitted elastic parameters do not gather any physical meaning with respect to the actual deflection on the real machine, though stiffnesses around motion axes revolve around the same values ($k_{z,1}$, $k_{z,2}$ and $k_{z,3}$) while normal stiffnesses ($k_{x,i}$ and $k_{y,i}$) are generally higher.

Next table Table 6 compares the fitted modal parameters to the measured ones using LMS Test.Lab. It is clear that the errors are higher when considering the raw measured FRFs since the multibody model is not able to handle non linear FRFs with non symmetric cross terms. Both the natural frequencies and the damping ratios are correlated with 40 % error. When the fitting occurs on the FRFs computed from [34], a slight increase on damping error is noticeable due to the underdetermined nature of the problem. Finally, the use symmetrized synthesized FRFs offers the lowest error in terms of fitting of natural frequencies but with a small increase of damping error.

MAC (modal assurance criterion) matrices, used to compare the mode shapes against the measured ones, are eventually displayed in Figure 11. Once again, it can be observed that when symmetrized synthesized FRFs are considered for the curve fitting, three of the four diagonal elements are increased, hence, reporting a higher correlation with measured mode shapes.

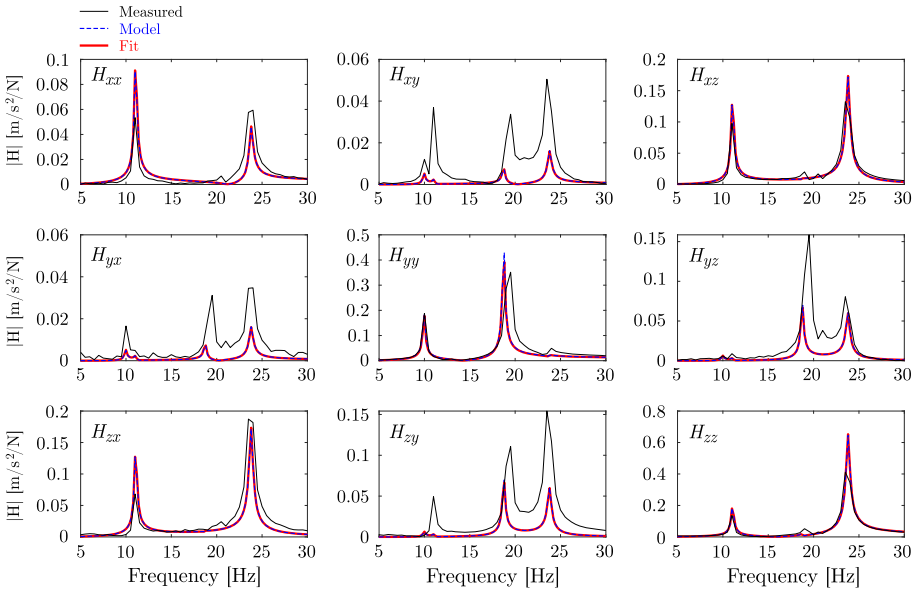

Fig. 7. FRF matrix $\mathbf{H}(\omega)$ fitted on parameters from [34]

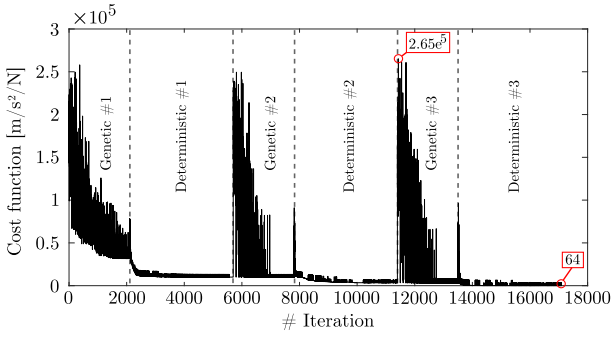

Fig. 8. Evolution of the cost function for the FRFs fitted on model parameters from [34]

Table 5
Comparison of fitted stiffnesses and dampings

	From [34]	Fit on model	Fit on measured FRFs	Fit on synthesized FRFs
$k_{z,1}$ [Nm/rad]	5.0e^6	5.0e^6	5.0e^6	3.5e^6
$k_{x,1}$ [Nm/rad]	6.1e^6	5.4e^6	5.8e^6	7.0e^6
$k_{y,1}$ [Nm/rad]	11.9e^6	15.4e^6	10.0e^6	11.9e^6
$k_{z,2}$ [Nm/rad]	6.9e^6	5.9e^6	8.0e^6	6.9e^6
$k_{x,2}$ [Nm/rad]	11.8e^6	11.3e^6	9.5e^6	22.6e^6
$k_{y,2}$ [Nm/rad]	8.1e^6	9.0e^6	32.0e^6	18.2e^6
$k_{z,3}$ [Nm/rad]	2.8e^6	2.8e^6	2.8e^6	2.7e^6
$k_{x,3}$ [Nm/rad]	5.2e^6	18.2e^6	100.0e^6	0.9e^6
$k_{y,3}$ [Nm/rad]	12.0e^6	23.3e^6	100.0e^6	21.01e^6
$d_{z,1}$ [Nm.s/rad]	0.02e^3	0.03e^3	0.12e^3	1.5e^3
$d_{x,1}$ [Nm.s/rad]	0.04e^3	0.6e^3	0.02e^3	0.001e^3
$d_{y,1}$ [Nm.s/rad]	3.1e^3	0.3e^3	0.006e^3	7.3e^3
$d_{z,2}$ [Nm.s/rad]	2.4e^3	2.6e^3	9.16e^3	0.4e^3
$d_{x,2}$ [Nm.s/rad]	0.04e^3	0.2e^3	0.01e^3	0.002e^3
$d_{y,2}$ [Nm.s/rad]	9.4e^3	10e^3	4.0e^3	0.3e^3
$d_{z,3}$ [Nm.s/rad]	0.2e^3	0.2e^3	0.03e^3	0.3e^3
$d_{x,3}$ [Nm.s/rad]	9.2e^3	4.1e^3	2.6e^3	0.08e^3
$d_{y,3}$ [Nm.s/rad]	0.08e^3	0.7e^3	9.0e^3	0.06e^3

6. Conclusion

A novel method for updating the elastic parameters of any flexible multibody model was presented at the dawn of Industry 4.0 aiming at generating digital twins to improve manufacturing processes. The updating method is based on a curve fitting of FRFs using a combination of genetic and deterministic algorithms. Synthesized FRFs in the sensor frame can directly be fitted without any transformation into the space of configuration parameters of the multibody model.

The application of the updating method on the elastic parameter identification can be summarized in four steps.

1. Perform an experimental modal analysis of the studied mechanical system by making sure that the sensor is located at a point experiencing high deflections. The structure must be excited at the sensor point to measure the FRFs of interest and also, at different locations (i.e. roving hammer) in order to capture the mode shapes.
2. Analyse the structural mode shapes and deduce the locations and orientations of the spring and damper pairs (e.g. for vertical machine tool, virtual elasticities can be inserted between the base and the column).
3. Build the kinematics of the multibody model based on the assumption of the locations of the spring and damper pairs. The dynamic model is built by knowing the inertial properties generally obtained using CAD models.
4. Apply the curve fitting method on the basis of the tooltip symmetrized and synthesized FRFs and the model derived at the previous step. Once the parameters of the genetic and deterministic algorithms are set, the routine is executed to provide optimal elastic parameters.

Table 6
Comparison of fitted modal parameters

	Measured	From [34]	Fit on model	Fit on measured FRFs	Fit on synthesized FRFs
f_1 [Hz]	10.0	10.0	10.0	11.0	10.0
f_2 [Hz]	11.0	11.1	11.1	11.2	11.1
f_3 [Hz]	19.2	18.7	18.7	19.5	19.5
f_4 [Hz]	23.7	23.8	23.8	24.0	23.6
$\text{Error}_{Average}$ [%]	/	17.5	17.5	40	12.5
ζ_1 [%]	1.4	1.1	1.0	1.6	0.9
ζ_2 [%]	1.0	1.0	1.0	0.3	1.0
ζ_3 [%]	0.5	0.6	0.6	0.1	0.7
ζ_4 [%]	0.8	0.8	0.8	0.5	0.8
$\text{Error}_{Average}$ [%]	/	10.0	12.5	40	17.5

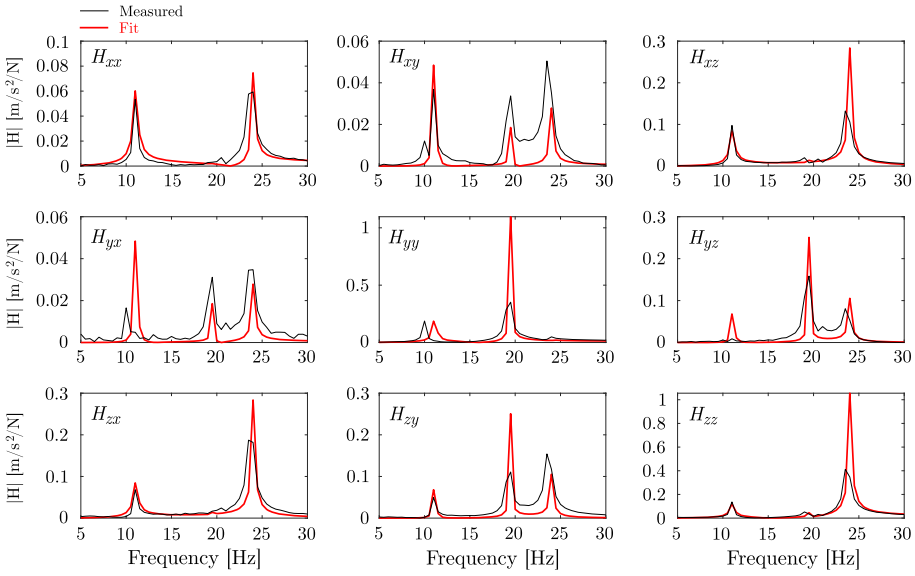

Fig. 9. FRF matrix $\mathbf{H}(\omega)$ fitted on measured FRFs in inertance format

The updating method was validated on a 3-DoF manipulator with known elastic parameters. The updating was able to find back the exact elastic parameters. Besides, the updating method was applied on industrial robot KUKA KR90 R3100 to find elastic parameters fitting the provided symmetrized synthesized FRFs. The method was also successfully used to determine elastic parameters for the Stäubli TX200 robot in the updating of the first ten modes [38]. Though, for robotic milling applications, it was reported that low-speed cutting mainly excites the first three joints while in high-speed milling, the spindle chatters [39]. The method can also be applied to vertical machine centers.

Nevertheless, as pointed out in [40], it is impossible to find a linear stiffness that perfectly matches the resonances for all positions when dealing with linear multibody model. Besides, the presented updating method provides elastic parameters in one posture, without physical meaning due to the underdetermined nature of the problem. Without considering the development of more sophisticated joint models, combining the actual deflection measurements estimating the joint stiffness could be used to guide the presented updating method. Applying the idea in several postures would potentially lead to the derivation of non linear stiffness and damping laws.

CRediT authorship contribution statement

Hoai Nam Huynh: Conceptualization, Formal analysis, Funding acquisition, Writing - original draft, Supervision. **Hamed Assadi:** Conceptualization, Writing - original draft. **Valentin Dambly:** Conceptualization, Investigation, Writing - original draft, Writing - review & editing. **Edouard Rivière-Lorphèvre:** Investigation, Writing - original draft, Writing - review & editing. **Olivier Verlinden:** Investigation, Writing - original draft, Writing - review & editing.

Declaration of Competing Interest

We wish to confirm that there are no known conflicts of interest associated with this, publication and there has been no significant financial support for this work that could have influenced its outcome.

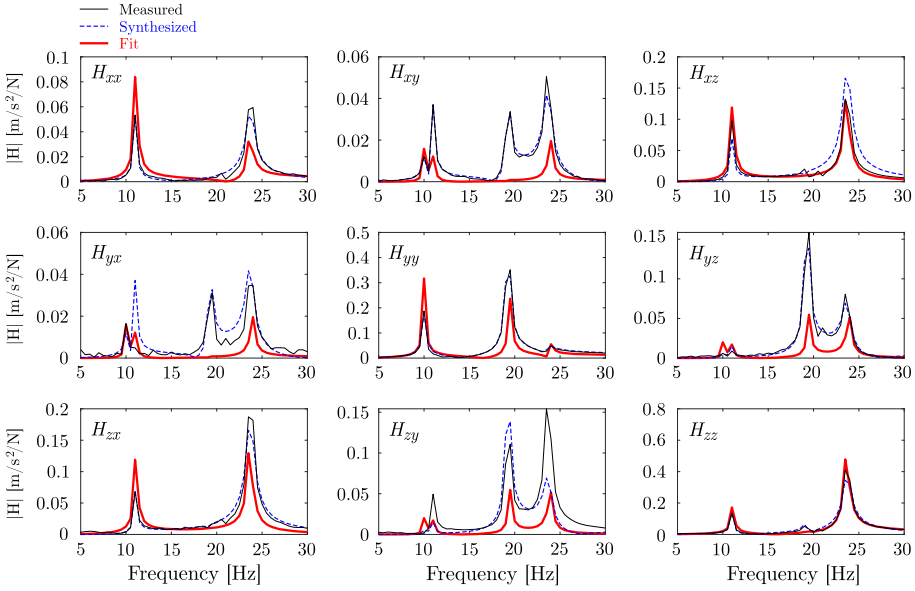

Fig. 10. FRF matrix $\mathbf{H}(\omega)$ fitted on synthesized FRFs in inertance format

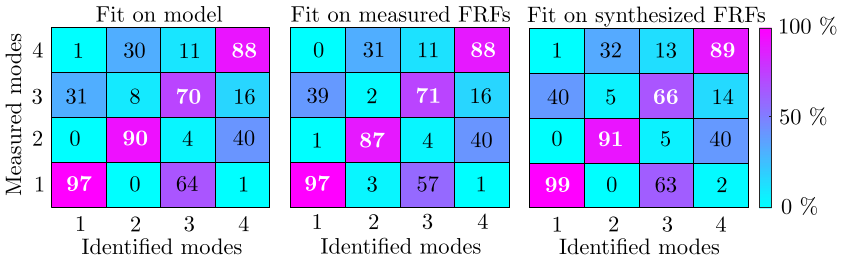

Fig. 11. MAC matrices from parameters fitted on model, measured and synthesized FRFs

We confirm that the manuscript has been read and approved by all named authors and that there are no other persons who satisfied the criteria for authorship but are not listed. We further confirm that the order of authors listed in the manuscript has been approved by all of us.

We confirm that we have given due consideration to the protection of intellectual property associated with this work and that there are no impediments to publication, including the timing of publication, with respect to intellectual property. In so doing we confirm that we have followed the regulations of our institutions concerning intellectual property.

We understand that the Corresponding Author is the sole contact for the Editorial process (including Editorial Manager and direct communications with the office). He/she is responsible for communicating with the other authors about progress, submissions of revisions and final approval of proofs. We confirm that we have provided a current, correct email address which is accessible by the Corresponding Author and which has been configured to accept email from hoainam.huynh@ubc.ca.

The authors declare that they have no known competing financial Interests or personal relationships that could have appeared to influence the work reported in this paper.

The authors declare the following financial interests/personal relationships which may be considered as potential competing interests.

Acknowledgement

The authors would like to acknowledge the Belgian National Fund for Scientific Research (NFSR) for the grant allotted to H.N. Huynh, and the University of Victoria (Canada) and Dynamic Optics for providing access to robot KUKA KR90 R3100 HA.

References

[1] E. Negri, L. Fumagallia, M. Macchia, A review of the roles of digital twin in cps-based production systems, Procedia Manufacturing, 11 (2017), pp. 939–948.
[2] M. Grieves, Digital Twin: Manufacturing Excellence through Virtual Factory Replication, Digital Twin White Paper, (2015).
[3] M. Armendia, M. Ghassempouri, E. Ozturk, F. Peysson, Twin-Control project, Twin-Control, Springer, (2018).
[4] S.H. Kim, E. Nam, T.I. Ha, S.H. Hwang, J.H. Loo, S.H. Park, B.K. Min, Robotic Machining: A Review of Recent Progress, International Journal of Precision Engineering and Manufacturing, (2019).
[5] I. Iglesias, M.A. Sebastian, J.E. Ares, Overview of the state of robotic machining: Current situation and future potential, Procedia Engineering 132 (2015) pp.911–917.
[6] W. Ji, L. Wang, Industrial Robotic Machining: A Review, International Journal of Advanced Manufacturing Technology, (2019), https://doi.org/10.1007/s00170-019-03403-z.
[7] A. Verl, A. Valente, S. Melkote, C. Brecher, E. Ozturk, L.T. Tunc, Robots in machining, CIRP Annals - Manufacturing Technology, (2019).
[8] H. Zhang, J. Wang, G. Zhang, Z. Gan, Z. Pan, H. Cui, Z. Zhu, Machining with flexible manipulator: Toward improving robotic machining performance, Proc. IEEE-ASME International Conference on Advanced Intelligent Mechatronics (USA, July, 2005) 1127–1132.
[9] P. Tavares, J.A. Silva, P. Costa, G. Veiga, A.P. Moreira, Flexible work cell simulator using digital twin methodology for highly complex systems in industry 4.0, Iberian Robotics conference, (2017), pp. 541–552.
[10] S. Makris, G. Michalos, G. Chryssolouris, Virtual Commissioning of an Assembly Cell with Cooperating Robots, Advances in Decision Sciences, Hindawi, 2012.
[11] P. Aivaliotis, K. Georgoulias, Z. Arkouli, S. Makris, Methodology for enabling digital twin using advanced physics-based modelling in predictive maintenance, Procedia CIRP, 81 (2019), pp. 417–422.
[12] Y. Altintas, M. Weck, Chatter stability in metal cutting and grinding, Annals of CIRP 53 (2004) 619–642.
[13] A. Klimchik, A. Ambiehl, S. Garnier, B. Furet, A. Pashkevich, Efficiency evaluation of robots in machining applications using industrial performance measure, Robotics and Computer Integrated Manufacturing, (2017).
[14] H.N. Huynh, E. Rivière-Lorphèvre, O. Verlinden, Multibody modelling of a flexible 6-axis robot dedicated to robotic machining, IMSD: Proceedings of the 5th Joint International Conference on Multibody System Dynamics, (Portugal, June, 2018).
[15] J. Swevers, C. Ganseman, D.B. Tükel, J. De Schutter, H. Van Brussel, Optimal Robot Excitation and Identification, IEEE Transactions on robotics and automation, 13 (1997), pp. 730–740.
[16] S. Mousavi, V. Gagnol, B.C. Bouzgarrou, P. Ray, Stability optimization in robotic milling through the control of functional redundancies, Robotics and Computer Integrated Manufacturing, (2018).
[17] O. Verlinden, H.N. Huynh, G. Kouroussis, E. Rivière-Lorphèvre, Modelling flexible bodies with minimal coordinates by means of the corotational formulation, Multibody System Dynamics, 42(4) (2018), pp. 495–514, https://doi.org/10.1007/s11044-017-9609-0.
[18] M. Cordes, W. Hintze, Offline simulation of path deviation due to joint compliance and hysteresis for robot machining, International Journal of Advanced Manufacturing Technology, 90 (2016), pp. 1075–1083.
[19] S. Mejri, V. Gagnol, Thien-Phu Le, L. Sabourin, P. Ray, P. Paultre, Dynamic characterization of machining robot and stability analysis, International Journal Advanced Manufacturing Technology, (2015), https://doi.org/10.1007/s00170-015-7336-3.
[20] J. Li, B. Li, N.Y. Shen, H. Qian, Z.M. Guo, Effect of the cutter path and the workpiece clamping position on the stability of the robotic milling system, International Journal of Advanced Manufacturing Technology, (2017), https://doi.org/10.1007/s00170-016-9759-x.
[21] C. Dumas, A. Boudelier, S. Caro, S. Garnier, M. Ritou, B. Furet, Développement d'une cellule robotisée de détourage des composites, Mécanique et industries 12 (2011) 487–494.
[22] T. Hardeman, Modeling and Identification of Industrial Robots Including Drive and Joint Flexibilities, University of Twente, 2008 Ph.D. thesis.
[23] J. Wang, H. Zhang, T. Fuhlbrigge, Improving Machining Accuracy with Robot Deformation Compensation, IEEE/RSJ International Conference on Intelligent Robots and Systems, (2011).
[24] H. Hage, Identication et simulation physique d'un robot Staubli TX90 pour le fraisage a grande vitesse, Universite Pierre et Marie Curie - Paris VI, 2012 Ph.D. thesis.
[25] C. Lehmann, B. Olofsson, K. Nilsson, M. Halbauer, M. Haage, A. Robertsson, O. Sörnmo, U. Berger, Robot Joint Modeling and Parameter Identification Using the Clamping Method, 7th IFAC Conference on Manufacturing Modelling, Management, and Control, (2013).
[26] G. Mercère, M. Lovera, E. Laroche, Identification of a flexible robot manipulator using a linear parameter-varying descriptor state-space structure, 50th IEEE Conference on Decision and Control and European Control Conference (CDC-ECC), 2011, http://folk.ntnu.no/skoge/prost/proceedings/cdc-ecc-2011/data/papers/0921.pdf.
[27] A. Karim, J. Hitzer, A. Lechler, A. Verl, Analysis of the Dynamic Behaviour of a Six-Axis Industrial Robot within the Entire Workspace in Respect of Machining Tasks, IEEE International Conference on Advanced Intelligent Mechatronics, (2017).
[28] M.F. Zaeh, O. Roesch, Improvement of the machining accuracy of milling robots, Production Engineering - Research and Development, (2014).
[29] F. Rafieian, Z. Liu, B. Hazel, Dynamic model and modal testing for vibration analysis of robotic grinding process with a 6dof flexible-joint manipulator, Proceedings of IEEE (2009).
[30] H.N. Huynh, G. Kouroussis, O. Verlinden, E. Rivière-Lorphèvre, Modal updating of a 6-axis robot for milling application, Proceeding of the 25th International Congress on Sound and Vibration, (July 2018).
[31] L. Zollo, E. Lopez, L. Spedaliere, N.G. Aracil, E. Guglielmelli, Identification of dynamic parameters for robots with elastic joints, Advances in Mechanical Engineering, (2014), https://doi.org/10.1155/2014/843186.
[32] A. Klimchik, D. Bondarenko, A. Pashkevich, S. Briot, B. Furet, Compliance error compensation in robotic-based milling, Lectures Notes in Electrical Engineering, (2014).
[33] C. Reinl, M. Friedmann, J. Bauer, M. Pischan, E. Abele, O. Von Stryk, Model-based Off-line Compensation of Path Deviation for Industrial Robots in Milling

Applications, IEEE/ASME International Conference on Advanced Intelligent Mechatronics, (2011).
[34] H.N. Huynh, H. Assadi, E. Rivière-Lorphèvre, O. Verlinden, K. Ahmadi, Modelling the dynamics of industrial robots for milling operations, Robotics and Computer-Integrated Manufacturing, 61 (2019).
[35] M. Neubauer, H. Gattringer, A. Müller, A. Steinhauser, W. Höbarth, A two-stage calibration method for industrial robots with joint and drive flexibilities, Mechanical sciences 6 (2015) 191–201.
[36] J.C. Lagarias, J.A. Reeds, M.H. Wright, P.E. Wright, Convergence Properties of the Nelder-Mead Simplex Method in Low Dimensions, SIAM Journal of Optimization, 9 (1998), pp. 112–147.
[37] A.E. Eiben, S.K. Smit, Evolutionary Algorithm Parameters and Methods to Tune Them, Autonomous Search, Springer, Berlin, Heidelberg, 2012, pp. 15–36. https://link.springer.com/chapter/10.1007/978-3-642-21434-9_2 .
[38] H.N. Huynh, Development and validation of a numerical model of robotic milling to optimise the cutting parameters, Ph.D. Thesis, University of Mons (Belgium), (2019).
[39] M. Cordes, W. Hintze, Y. Altintas, Chatter stability in robotic milling, Robotics and Computer Integrated Manufacturing, 55 (2019), pp. 11–18, https://doi.org/10.1016/j.rcim.2018.07.004.
[40] E. Wernholt, S. Moberg, Frequency-Domain Gray-Box Identification of Industrial Robots, Proceedings of the 17th World Congress The International Federation of Automatic Control, (2008).